Theoretical Predictions of EM-induced Degradation in Test-Structures and On-Chip Power Grids with Analytical and Numerical Analysis

Valeriy Sukharev, Armen Kteyan, and Jun-Ho Choy
Mentor Graphics Corporation, D2S
Fremont, CA 94538, USA
Phone: (1) – (510)-354-5531, Valeriy_sukharev@mentor.com

Sandeep Chatterjee and Farid N. Najm
Electrical and Computer Engineering
University of Toronto
Toronto, Ontario, Canada M5S 3G4

***Abstract*—Paper discusses the state of the art physics-based analytical modeling and numerical analysis techniques developed for the prediction and description of electromigration (EM) induced conductance degradation of individual interconnect metal lines and on-chip power grids. Mechanical stress evolution caused by an electric current driven redistribution of vacancies and plating atoms, which populate the metal grain boundaries (GB) and interfaces, initiates the growth of preexisted crystal imperfections such as micro cavities and interfacial/inter-granular delaminating. It is described as a major cause of the failure. A role in the failure development played by the interfacial and GB atomic diffusions and their variation is covered. A close relation between the interfacial-adhesion energy and so-called "critical stress" is clarified. A physics-based statistical formulation of EM phenomenon is discussed.**

Different kind of analytical/numerical techniques employed for analysis of EM degradation in different cases characterized by the scales varying from the size of an individual line to the multibillion segment power grids are discussed. Conditions for employment of 1D EM approximation (Korhonen's equation) are validated by direct comparison with results of 3D FEA simulations. Implementation of the novel compact model- and FDA-based approaches for analyzing EM-induced IR-drop degradation in power nets is demonstrated.

***Index Terms*—Electromigration, reliability, diffusion, on-chip interconnect, power grid, test-structures.**

I. INTRODUCTION

Ever increasing interconnect current density due to continuous reduction in critical dimensions of the advanced technology nodes makes EM assessment as one of the most important design sign-off checks. An employment of FinFET devices in chip design adds additional concerns about the increase in chip electric current density and acceleration of the age-induced failures rates. Excessive Joule heat generation caused by elevated current densities makes the development of these failures even faster. Nevertheless, modern semiconductor chips, while working in the range of elevated current densities and temperatures, should satisfy the scope of strict reliability requirements. One of them is a requirement of 10 year chip immortality, which is the same as for the elder generation chips. To satisfy this requirement the chips should be designed in accordance with a special set of design rules and practices. A well-known conservatism of these rules results in the problems with chip performance. In order to understand the source of this conservatism we should examine the methodology employed for these design rules generation. As we know the major EM problem is a degradation of the circuit electrical characteristics. It can result in both the short and open circuits. Voids generated in the metal can be responsible for the resistance increase, and, in the worst case, for the open circuit. Hillock formation, which is a metal extrusion into an inter-metal isolation, can form shorts between the neighboring wires. A standard EM testing is performed on Cu lines connected to a lower or upper metal levels by vias. The electric current flows from wide metal supply lines through the vias into the test line. The changes in the voltage and resistance taking place with the duration of time are detected. Increase in resistance of the individual line above the threshold value is considered as a failure. Details describing this methodology characterized by a variety of measurement techniques were published in many papers, see for example [1]. Despite the deference in implementations of the testing procedure, the determination of failure is the same: a multilink structure of the conducting wires is failed when any single wire is failed (the series failure mode). While being valid for estimation of the time to failure (TTF) of an individual wire, and the mean time to failure (MTTF), after a corresponding averaging procedure is performed on a set of the identical wires, this failure mode does not describe well the failure of a large electrical circuit where nodes form a grid-like structure. A redundancy for the current conductance existing in such circuits is responsible for the sustain operability even when some fraction of individual wires were failed. It's known that the electrical connectivity between opposite sides of an electrical net characterized by a mixture of sequentially or parallel connected current conducting segments will not be broken till a critical fraction of the segments, so-called percolation threshold, will be cutoff. This threshold fraction depends on the net dimension, structure, and size [2]. The on-chip interconnect power-ground

(p/g) grids of the modern semiconductor chips are similar to such nets. The failure criterion for the p/g grid is of course not a complete cutting off the electrical conductance but a development of the voltage drop exceeding the threshold drop specified by a designer. This threshold voltage drop means a critical reduction in the supply voltage (Vdd/Vss) happening somewhere in the layout at the particular gate, which destroys the proper cell functionality.

Hence, the accepted failure criteria depend on a scale of the analyzed problem migrating from the simple threshold increase in the resistance of an individual line (wire) to the threshold increase in the voltage drop in the case of large circuits. It should be stressed out that while the failure criteria are different, the physical mechanism causing the failures is the same. It is an increase in the resistance of individual wires caused by EM induced voiding. Thus, in order to accomplish the EM assessment we should have a capability to calculate the EM induced resistance change of each and every single wire of the p/g grid at any instance in time. Since the dynamics of EM-induced resistance change is caused by a void nucleation and growth, the physics-based modeling technique providing a circuit-wide distribution of the void nucleation times and void growth kinetics should be available. Majority of the EM assessment models described in literature are empirical, derived on the basis of the fit with available experimental data [3]. They are not allowing to take into account many important physical details that affect the metal degradation occurring when electrical stressing is applied. These are the grain size and texture determining the GB atom/vacancy diffusivity, residual stress, etc. effecting the void nucleation and growth.

It is obvious that problems characterized by different scales can afford quite different level of details, which can be included in the predictive modeling. For example, the role played by a particular grain size distribution and a texture in the EM induced stress evolution can be addressed by the finite-element analysis (FEA) performed on the individual interconnect test-structure, [4], and cannot be addressed (with the same level of accuracy) by the one-dimensional (1D) simulation of the stress evolution in the interconnect trees or p/g grids.

A primary target of this paper is demonstrating some of the recently developed models, discussing the ranges of applicability of different modeling approaches, and the ways of implementation of different kind of numerical and analytical techniques for the EM assessment.

The reminder of the paper is organized as follows. In Section II we present some background material regarding EM, a general model of the evolution of vacancy and plated atom concentrations and stress under the action of electric stressing. Employment of the phase-field method for description of void evolution is discussed. Sections III and IV deal with 1D approximation of EM phenomenon and its comparison with 2D/3D models. Section V demonstrates the employment of 1D approach for EM assessment of large p/g grids. Section VI concludes the paper.

II. Phenomenological Model of EM

A. EM-Induced Atomic Perturbation

As it is agreed, the EM phenomenon is the directional migration of lattice atoms and defects under the action of the electric field and current. This forced redistribution of atoms can generate non-uniformity in chemical composition, and can introduce non-uniform elastic/plastic deformation and stress. Directional migration of atoms in solids can happen under the action of oriented forces only. These forces, which are proportional to the gradient of the potential energy $F(\vec{r}) = -\nabla U(\vec{r})$, push atoms to migrate along this gradient with the velocity $\vec{v} = \mu F(\vec{r})$. The coefficient proportionality μ, representing the atom mobility, relates to the atomic diffusivity D_a through the Einstein relation, [5]: $D_a = \mu k_B T$, where, k_B and T are the Boltzmann constant and absolute temperature. The state of equilibrium is achieved when a balance between the tendency of atoms to migrate toward the lower potential energy $U(\vec{r})$ and their tendency to spread out due to the thermal diffusion is established, or, in other word, when the total atomic flux is vanished. Describing the atomic flux $\Gamma(\vec{r})$ as a number of atoms crossing the unit surface normal to the direction of the atomic flow per unit time, we can write:

$$\Gamma(\vec{r}) = \mu F(\vec{r}) N_A(\vec{r}) = -N_A(\vec{r}) \frac{D_a}{k_B T} \nabla U(\vec{r}) \qquad (1)$$

Here, $N_A(\vec{r})$ is the coordinate dependent atomic concentration.

Potential energy of a lattice atom depends on a number of physical factors such as the temperature, chemical composition, mechanical stress, electrical field, etc. Variation in $U(\vec{r})$ caused by variations of these parameters can initiate the matter redistribution. For example, when an electric field is applied to the metal body (wire, film, etc.), the atomic flux caused by the combined interaction between metal ions and electric field and conduction electrons flows toward the anode, and is described as

$$\Gamma_{EM}(\vec{r}) = -N_A(\vec{r}) \frac{D_a}{k_B T} eZ^* \rho j(\vec{r}) \qquad (2)$$

Here, Z^* is the, so-called, effective valence, which depends on the metal properties, [6], $\rho(\vec{r})$ is the metal resistivity and $j(\vec{r})$ is the current density.

When the electric current passes through the metal wire it generates the volumetric strain caused by the atom density redistribution. In the case of a metal line confined by a rigid surrounding this volumetric strain generates nonuniform distribution of the hydrostatic stress along the wire. As a result, an additional atom migration is caused by the action of forces generated by an inhomogeneity of elastic energy accumulated in the lattice. The change in the free energy of the regular lattice atom caused by the presence of the hydrostatic stress σ_{Hyd} is described as, [7]:

$$\Delta U(\vec{r}) = U_{hyd}(\vec{r}) = -\Omega \sigma_{Hyd}(\vec{r}) \qquad (3)$$

Here, Ω is a volume occupied by a lattice atom, and the hydrostatic stress σ_{Hyd} is the mean of the sum of normal stress components. It can be understood as a work done by this stress when an extra volume of Ω is created inside a confined wire. Thus, the atomic flux caused by an inhomogeneous distribution of the hydrostatic stress can be presented as

$$\Gamma_\sigma(\vec{r}) = N_A(\vec{r})\frac{D_a\Omega}{k_B T}\nabla\sigma_{Hyd}(\vec{r}) \tag{4}$$

An additional atomic flux generated by an inhomogeneous distribution of the atom concentration is

$$\Gamma_N(\vec{r}) = -D_a\nabla N_A \tag{5}$$

It should be mentioned that the Soret diffusion is not considered in this paper.

Now we need to understand how a redistribution of the atomic density can result in an electrical degradation of the metal. A redistribution of the atomic density is accompanied by generation of the volumetric deformation. When a metal wire is embedded into a rigid confinement, which is the case of the interconnect metallization, the dilatation generates the stress. Over time, the lasting unidirectional electrical load

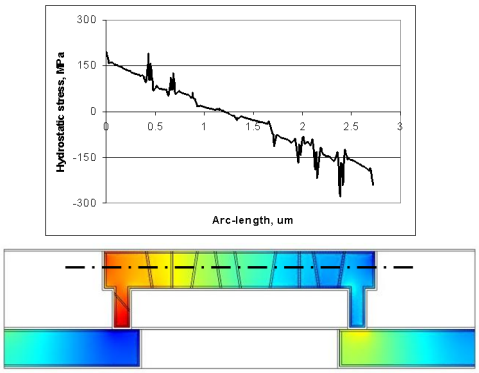

Fig. 1 EM-induced distribution of the hydrostatic stress along the dot-dashed line, [8].

increases these stresses, as well as the stress gradient along the metal line, Fig. 1. This stress can reach a critical level, resulting in a void nucleation at the cathode and/or hillock formation at the anode ends of line, which affect interconnect electrical characteristics. EM-induced generation of hillocks and corresponding development of the electrical shortages is not considered in this paper due to its infrequent nature. In the case of voiding, existing cohesive or interfacial micro-cracks located near or at the Cu/dielectric cap or Cu/barrier interfaces can be developed into voids by an action of the appropriate stresses. The physical meaning of the introduced critical stress responsible for void nucleation has been intensively discussed, see for example [9, 10, 11].

An estimation of the σ_{crit} on the basis of the classical model of the homogeneous nucleation can be found in [10, 11]. Assuming that a void can be nucleated only when a pre-existing flaw exists, it was concluded that the flaw with the initial size r_f will start growing if the surrounding stress exceeds the value of $\sigma_{crit} = 2\gamma/r_f$, where γ is the surface energy per unit area.

Thus, assuming a variation in sizes of the void precursors we can come out with a range of critical stresses, which means that a growth of a particular precursor will start when the stress generated by electric current will reach the corresponding level. Thus, the so-called void nucleation is getting a clear statistical nature: void initiation depends on locations and sizes of the pre-existing defects. This can explain a poor EM performance traditionally observed at the early stages of new technology development when the metal interfaces are not optimized yet. It also corresponds well to the observations made in [12] of the correlation between the EM resistance and adhesion properties of the metal interfaces.

B. Evolution of the Vacancy Concentration caused by EM

In order to create a formalism describing the stress evolution we need, first, to extract the atom concentration evolution, and, second, to generate a link between the changes of atom concentration and stress. The first task can be easily accomplished by solving an appropriate continuity equation coupling the rate of evolution of the local atomic concentration $N_A(\vec{r},t)$ with the atomic flux divergence occurring at this particular location $\vec{r}$

$$\frac{\partial N_A(\vec{r},t)}{\partial t} + \vec{\nabla}\Gamma_A(\vec{r},t) = 0, \tag{6}$$

where $\Gamma_A(\vec{r},t)$ is the total atomic flux described by a combination of fluxes given by (1)–(5) at the location $\vec{r}$, at the instance in time t. It is known, [6], that typical interconnect metals such as Al and Cu are characterized by the vacancy mechanism of diffusion. It means that an atomic diffusivity depends on the vacancy concentration, which, in turn, is a function of the temperature and hydrostatic stress. Since the flux of atoms equals to the vacancy flux but is oriented in an opposite direction, a modeling of the vacancy diffusion can be used instead of atomic diffusion. A vacancy diffusivity is represented by the standard Arrhenius form

$$D = D_{V0}\exp\left\{-\frac{E_{VD} - \Omega^*\sigma_{Hyd}}{kT}\right\} \tag{7}$$

Here, E_{VD} is the activation energy of the vacancy diffusion, which is a sum of the energy of vacancy formation and the energy required for diffusing atom to be moved from its initial site to the saddle point (activated complex), $E_{VD} = E_V + E_D$, [13]. $\Omega^* \approx 0.95\Omega$ is a combination of the vacancy formation volume, which is the crystal volume change upon formation of a vacation in its standard state, and the migration volume, which is the additional volume change when the defect reaches the saddle point in its migration path, [14]. EM induced fluxes of vacancies are described by expressions (2)-(5) where the atomic concentration and diffusivity are replaced by the vacancy concentration $N(\vec{r})$ and diffusivity $D(\vec{r})$, and Ω is replaced by the $(1-f)\Omega$, where $f = \Omega_V/\Omega$, which is the ratio of the vacancy and atomic volumes. A polycrystalline structure of interconnect metals introduces additional complications to

the description of the matter transfer. Indeed, metal interfaces (IF) and GBs are characterized by much faster atomic diffusivities then grain interiors. We are describing this well-known effect by introducing the lower energies for vacancy formation and diffusion at the IFs and GBs in comparison with grain bulks.

Stressing the solid with different types of loads (electrical, mechanical, thermal) disturbs the state of thermo-chemical equilibrium of the lattice defects. A system evolves to a new state of equilibrium corresponding to new conditions. It is known that an infinite crystalline solid in the state of zero stress condition is characterized by a thermally equilibrium concentration of vacancies: $N_0^{ZS} = \Omega^{-1} \exp\{-E_V / k_B T_{ZS}\}$, where E_V is the energy of vacancy generation, T_{ZS} is the temperature corresponding to the state of zero stress condition, and Ω^{-1}, is the density of lattice sites. The presence of stresses yields the new equilibrium vacancy concentration equals to:

$$N^{eq} = \exp\left\{-\frac{E_V - f\Omega\sigma_{Hyd}}{k_B T}\right\} = N_0(T)\exp\left\{\frac{f\Omega\sigma_{Hyd}}{k_B T}\right\} \qquad (8)$$

Here and everywhere below the vacancy concentration is expressed as a fraction of the lattice sites density Ω^{-1} not occupied by atoms. A presence of the multiplier f in (8) can be explained by the work that should be done against the hydrostatic stress for the vacancy formation. It includes the work done against pressure when a lattice atom transferred to the GB or IF deforms its thicknesses: $\Omega\sigma_{Hyd}$, and the work performed during the volume relaxation around the newly formed vacancy: $-(1-f)\Omega\sigma_{Hyd}$.

Mechanism of the transition to the new state of equilibrium distribution of vacancies consists of two independent steps: vacancy generation-annihilation and vacancy diffusion. Formation of an extra vacancy at the lattice site is accompanied by removing a lattice atom occupying this site to any place in the solid where the regular lattice structure is destroyed: IFs with a confinement, GBs, dislocation edges, etc. Atoms transferred to IFs or GBs can build (plate) a continuation of the grain lattices. These atoms also can, when placed on the dislocation edges, cause its climb. Vacancies can be formed inside the very top layer of the grain interior, from where the "vacancy generating" atoms are transferred to the inhomogeneous surfaces and interfaces. Thus, the energy of vacancy formation cannot be calculated independently from the formation energy of the paired species.

Hence, an additional continuity equation describing the evolution of the paired species concentration $M(\vec{r},t)$, which we called "plated atoms", should be added:

$$\frac{\partial M}{\partial t} + G = 0 \qquad (9)$$

with the generation-annihilation term equals to

$$G = \frac{N - N^{eq}}{\tau} \qquad (10)$$

Here, N is the concentration of vacancies in GB/IF, N^{eq} is the GB/IF equilibrium vacancy concentration (8), and τ is the appropriate time constant. In equation (9), a sink/source term G is introduced in order to describe the vacancy/plated atom pair generation/annihilation kinetics, which takes place at GBs/IFs. Because of the big difference in mobility of atoms and vacancies we expect plating atoms to stay where they were generated inside interfaces and GBs, while vacancies should migrate under the action of various driving forces. It should be mentioned that the phenomenon of the additional volume generation/disappearance due the pair formation/annihilation has been accounted by Kirchheim [15], and Sarichev et al. [16] by introducing an additional volume evolution equation. In our approach it is described by the introduced plated atom kinetics. The same sink/source term G should exist in the continuity equation for evolution of vacancy concentration at the GB/IF:

$$\frac{\partial N}{\partial t} + \vec{\nabla}(-D_{IF/GB}\vec{\nabla}N - \frac{D_{IF/GB}N}{k_B T}(1-f)\Omega\vec{\nabla}\sigma_{Hyd} - \\ - \frac{D_{IF/GB}N}{k_B T}eZ^*\rho j) + G = 0 \qquad (11)$$

Here, $D_{IF/GB}$ is vacancy diffusivity in the GB/IF. Evolution of the vacancy concentration inside grain bulks is described by the equation similar to (11) with omitted generation/annihilation term:

$$\frac{\partial N}{\partial t} + \vec{\nabla}(-D\vec{\nabla}N - \frac{DN}{k_B T}(1-f)\Omega\vec{\nabla}\sigma_{Hyd} - \frac{DN}{k_B T}eZ^*\rho j) = 0 \qquad (12)$$

Here, D is the vacancy diffusivity in the grain interior.

The sink/source term G in (13) is the same as in equation (11) describing the evolution of the vacancy concentration in GB/interface, which is in line with the assumption of simultaneous generation/recombination of the vacancy and plated atom, i.e. vacancy - plated atom pair.

C. Linking with the Stress

In this section, we will demonstrate a way how to calculate the stress distribution based on known distributions of vacancies and plated atoms i.e. the distribution of the inelastic volumetric strain. This formalism is similar to the methodology of thermal stress calculation developed by Landau and Lifshitz, [17]. If the concentrations of vacancies and plated atoms are changed in any way then, even in the case of absence of external forces and the uniform temperature, the solid body will be deformed on account of the dilatation effect.

A change in the vacancy concentration occurs as a result of the generation or annihilation of vacancy-plated atom pairs and the diffusion of vacancies. Both these steps result in a local volume change. Because of a difference between the vacancy volume Ω_v and the atomic volume Ω, a vacancy generation and annihilation results a dilatational volume strain $e_v = ((\Omega_v - \Omega)/\Omega)\Delta N = -(1-f)\Delta N$. Here, $\Delta N = N - N^{ZS}$ is a change in vacancy concentration. Thus, for the vacancy-induced strain we have $\varepsilon_v = e_v/3 = -(1-f)\Delta N/3$. Dilatation caused by the atom plating we describe as generation or

removal of an extra volume Ω in the GBs and/or interfaces. Thus, the total volume strain can be described as:

$$\theta = -(1-f)\Delta N + M. \tag{13}$$

It should be mentioned, that ΔN and ΔM in (13) are not necessarily equal each other. A standard derivation provides us with the following expression for the stress components

$$\sigma_i = \lambda e + 2G\varepsilon_i - \frac{E}{3(1-2\nu)}(M-(1-f)\Delta N) \tag{14}$$

where the Lame coefficient λ and the shear modulus G have the form: $G = E/2(1+\nu)$ and $G = E/(1+\nu)(1-2\nu)$. Here, E and ν are the Young's modulus and the Poisson's factor. Substituting σ_i from (14) into the partial differential equation (PDE) for force balance, [18], and assuming absence of the body forces, we can find:

$$(\lambda+G)\frac{\partial e}{\partial x_i} + G\Delta u - \frac{E}{3(1-2\nu)}\left(\frac{\partial M}{\partial x_i} - (1-f)\frac{\partial N}{\partial x_i}\right) = 0 \tag{15}$$

where the terms

$$X_i = -\frac{E}{3(1-2\nu)}\left(\frac{\partial M}{\partial x_i} - (1-f)\frac{\partial N}{\partial x_i}\right) \tag{16}$$

$$X_i = \frac{E(1-f)}{3(1-2\nu)}\frac{\partial N}{\partial x_i} \tag{17}$$

take place of the body force components in GB/IF and grain interiors correspondingly. Conditions of the equilibrium at the surface of the solid body with the vacancies and plated atoms yield the following surface force balance PDE

$$\frac{E}{3(1-2\nu)}(M-(1-f)\Delta N)l = \lambda e l + G\left(\frac{\partial u}{\partial x}l + \frac{\partial u}{\partial y}m + \frac{\partial u}{\partial z}n\right) + \\ + G\left(\frac{\partial u}{\partial x}l + \frac{\partial v}{\partial x}m + \frac{\partial w}{\partial x}n\right) \tag{18}$$

where the terms

$$Y_i = \frac{E}{3(1-2\nu)}(M-(1-f)\Delta N)n_i \tag{19}$$

take place of the surface force components.

Thus, the displacements u_i generated by vacancies and plated atoms distributed in the GBs, and IFs are equal to the displacements produced by the body forces (16) and (17) for the body forces in grain interiors, and by the tension (19) distributed over the solid body surface. From the equation (14) we can see that the normal stress components consist of two parts, a "traditional" elastic part, which is derived by using elastic strain/stress relations, and the inelastic part describing the dilatational-induced pressure of the amount of:

$$\Delta P_{IF/GB} = -\frac{E}{3(1-2\nu)}(M-(1-f)\Delta N), \\ \Delta P = \frac{E(1-f)}{3(1-2\nu)}\Delta N \tag{20}$$

for the GBs/IFs, and grain interiors, which are proportional to the concentrations of vacancies and plated atoms.

Thus, the EM-induced stress evolution inside an arbitrary taken interconnect segment can be obtained by a solution of the system of coupled second order PDE. These are the continuity equations (9)-(12) describing the evolution of the concentrations of vacancies and plated atoms, the force balance equations (15) for all three components of the displacement, and the Laplace's equation for the current density distribution everywhere inside the segment. In general case this system can be solved numerically by employing the FEA technique. Using appropriate boundary conditions (BC) for all involved modules such as zero flux conditions for the metal-barrier interfaces in the continuity equations, zero displacements for the interfaces with the rigid confinement in the force balance equation, and the isolation, voltage or current sources BC for the Laplace's equation allows us to get physically viable solutions for many cases. Fig. 1 demonstrates the hydrostatic stress distribution along an upstream electron

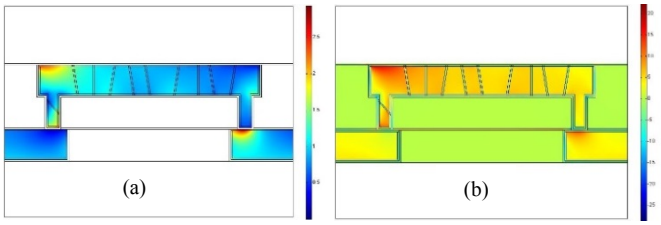

Fig. 2. Distributions of vacancies - (a), and hydrostatic stress - (b) in the test-structure with the electron flow coming through left up-stream via and the crystallography dependent Young's modulus.

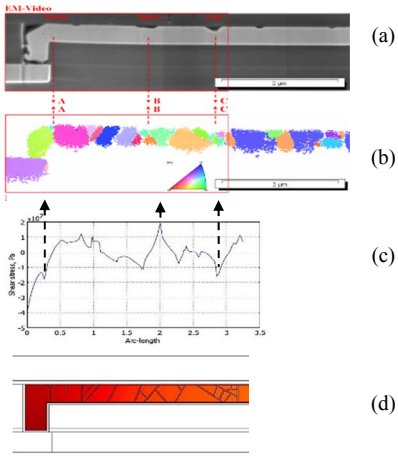

Fig. 3. Postmortem SEM/EBSD analysis of sample (I) and simulation results: (a) SEM image of the cross section of Cu sample together with (b) an IPF map (EBSD measurement) of the crystallographic orientation of the individual grains relative to the wafer surface; (c) simulated distribution of the shear stress at the top copper/dielectric barrier interface for copper line, with the grain structure shown in (d), [4].

flow test structure. Figures 2 and 3 show the distributions of vacancies and hydrostatic stress in the polycrystalline test structure with grains characterized by different crystallography orientations relative the line direction, and the correlation between the interfacial shear stress distribution, caused by the anisotropy in mechanical properties of polycrystalline copper line, and the voiding locations.

D. *Void Growth and Postvoiding Stress Evolution*

The described above formalism predicts the stress evolution occurring in the interconnect segment loaded with electric current until the voiding is started.

Origination of a free surface inside the metal line due to void nucleation can be described by means of the phase-field approach [19]. A phase field ϕ (also called an order parameter) describes the void and metal regions as two different phases in a way that all material properties such as metal conductivity, Young's modulus, diffusivity of vacancies, etc. are vanished inside the void. This is achieved by the following phase-field definition

$$\begin{aligned} \phi &= 1 \quad in\ metal \\ \phi &= -1 \quad in\ void \end{aligned}, \tag{21}$$

which provides the following representation of the materials and transport properties everywhere inside the metal

$$\eta = \frac{1+\phi}{2}: \ \gamma_\phi = \gamma\eta, \ E_\phi = E\eta, \ D_\phi = D\eta \tag{22}$$

The model provides a smooth transition between the two phases by corresponding smooth behavior of ϕ in a narrow region δ representing the void-metal interface. Evolution of the order parameter ϕ is described by the non-linear equation:

$$\frac{\partial\phi}{\partial t} - \xi^2\nabla^2\phi + \left(\phi^2 - 1\right)\phi + V\nabla\phi = f(\sigma) \tag{23}$$

where the parameter ξ defines the interface thickness $\delta = \sqrt{2\xi}$ and V is the rate of surface motion. Right-hand term in (23) allows to introduce void region in the initially void-less metal, when the EM-induced stress achieves σ_{crit}:

$$f\left(\sigma_{Hyd}\right) = -f_0 \cdot (\phi+1) \cdot \left\{ \begin{matrix} 0, if\ \sigma_{Hyd} < \sigma_{crit} \\ 1, if\ \sigma_{Hyd} \geq \sigma_{crit} \end{matrix} \right\} \tag{24}$$

The duration of nucleation process is controlled by the parameter f_0; the term (24) vanishes when ϕ achieves new equilibrium state $\phi = -1$. The velocity of the void surface motion is determined by the vacancy inflow flux from the metal bulk directed normal to the surface, and by the divergence of the flux of vacancies migrating along the void surface:

$$V = \Omega\left(-\nabla J_s + J_n\right) \tag{25}$$

Here, $J_n = -\frac{D}{k_B T}\left(\nabla\sigma + \frac{eZ^*\rho j}{\Omega}\right)$ and $J_s = -\frac{D_s}{k_B T}\nabla\mu_s$, where D_s is the surface diffusivity. The chemical potential $\mu_s = \gamma\xi\nabla^2\varphi + \frac{\partial W}{\partial\varphi}$, is determined by the surface energy γ and by variation of strain energy $W(\varepsilon,\varphi)$ along the surface, [19].

Since the inflow of vacancies into the growing void is a major factor effecting the void shape evolution, the grain microstructure providing the distribution of GB around the void plays crucial role in void shaping. Fig. 4 demonstrates the void evolution taking place when GBs are uniformly distributed around the growing void – (a), and when a single GB crossing the week top interface provides a venue for the fast vacancy migration – (b).

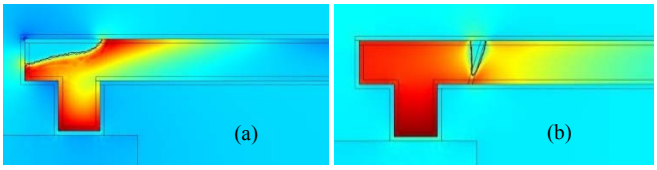

Fig. 4. Void evolution in a case of uniform distribution of GB in the near void region, (a), and the effect of a single GB on a void evolution, (b).

As an additional demonstration of the simulation capabilities, Fig. 5 demonstrates the simulated drift of the line edge caused by a DC current applied to the Blech strip test structure of EM.

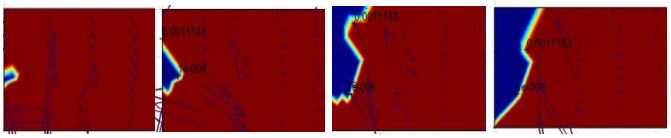

Fig. 5. Line edge drift in the Blech strip test structure of EM, [20].

III. 1-D Approximation of EM-Induced Degradation

The described above comprehensive model of the EM-induced degradation in an arbitrary segment of on-chip interconnect can be helpful in designing the test structures of EM, and in interface and texture engineering. But the complexity of this model, which requires an employment of the advanced numerical methods, restricts its usability just for the cases of relatively small sizes. It cannot help to address EM-induced degradation in large VLSI electric circuits such as interconnect p/g grids. As a possible solution, we can consider an employment of simpler 1D models. Such models while demonstrating short runtimes nevertheless should keep all essential physical features of the EM phenomenon. Here, we will demonstrate 1D EM approximation obtained by reduction of the described above full EM model.

A number of attempts have been undertaken to develop such 1D approximation, [9, 15, 21]. In all these 1D approximations a kinetics of stress evolution occurring in the confined and electrically loaded metal line was resolved by employing a simple relation between the volumetric strain θ and the hydrostatic stress

$$\sigma_{Hyd} = -B\theta \tag{26}$$

Here, B is the effective bulk modulus, and θ is the volumetric strain. Variation in θ is originated by redistribution of the lattice atoms along the line caused by the electron wind and by the equilibration of the vacancy concentration with the stress. The introduced effective bulk modulus B should effectively describe an interaction between volumetrically deformed line and confinement; see for example [22].

A major challenge for such approaches is an accurate calculation of the volumetric strain θ and stress generated by interaction with confinement. As it was demonstrated above, the inelastic volume strain generated in an unit volume by vacancy migration is $\theta_{vm} = \left(\left(\Omega_v - \Omega\right)/\Omega\right)\Delta N_m = -(1-f)\Delta N_m$,

and by vacancy/plated atom generation/annihilation is $\theta_{vg} = \Omega^{-1}\left(\Omega M + (\Omega_V - \Omega)\Delta N_g\right) = M - (1-f)\Delta N_g$, where $M = -\Delta N_g$. Here, ΔN_g and ΔN_m are the vacancy concentration changes caused by generation/annihilation and migration. Thus, a total vacancy change is $\Delta N = \Delta N_g + \Delta N_m$, and a total inelastic volume strain is described by (13). It should be mentioned that if not for a confinement, this inelastic volume change would certainly occur. Since the rigid confinement doesn't allow the metal volume changing, the generated elastic stress demonstrates a sign, which is opposite to the sign of inelastic strain.

Introducing the effective diffusion coefficient and effective generation/annihilation rate, the both are averaged on the entire cross section of the line, [9, 10], the considered above system of PDEs can be reduced to 1D case

$$\begin{aligned} &\frac{\partial N}{\partial t} + \frac{\partial}{\partial x}\left[-\frac{DN}{k_B T}\left((1-f)\Omega\frac{\partial \sigma}{\partial x} + \frac{eZ^*\rho j}{\Omega}\right)\right] = -G \\ &\frac{\partial M}{\partial t} = -G \\ &\sigma = B\left((1-f)\Delta N - M\right) \end{aligned} \tag{27}$$

Accepting Korhonen's assumption of the very fast equilibration of the vacancy concentration with the stress, i.e. assuming the validity of: $\Delta N = N^{eq} - N_0^{ZS}$, we obtain

$$\frac{\partial \Delta N}{\partial t} = \frac{f\Omega}{kT} N^{eq}\frac{\partial \sigma}{\partial t} \tag{28}$$

Combining together the equations (26)-(28), we come to the following equation

$$\frac{\partial N}{\partial t} + G = \frac{\partial \Delta N}{\partial t} - \frac{\partial M}{\partial t} = \left(\frac{1}{B} + \frac{f\Omega}{kT} N^{eq}\right)\frac{\partial \sigma}{\partial t} \tag{29}$$

Assuming a validity of the approximation $B\Omega f N^{eq}/k_B T << 1$, which is same that was used in [9], and recalling that the atomic diffusivity is determined as $D_a = (1-f)DN$, the equations (29) and (28) yield the Korhonen's equation

$$\frac{\partial \sigma}{\partial t} = \frac{\partial}{\partial x}\left[\frac{D_a B\Omega}{k_B T}\left(\frac{\partial \sigma}{\partial x} + \frac{eZ^*\rho j}{\Omega}\right)\right] \tag{30}$$

Hence, making exactly same assumptions, which were made in [9] for development of the equation (30), we were able to reduce our full multiphysics EM model to the same 1D representation. Below we will demonstrate some results obtained with this 1D approximation.

A solution of (30) for the case of the wire of length L with diffusion blocking ends loaded with DC current density j provides the well-known kinetics of stress evolution, [9]

$$\begin{aligned} &\sigma(x,t) = \sigma_T - Gx + \frac{GL}{2} - 4GL\sum_{k=0}^{\infty}\frac{\cos\{(2k+1)\pi x/L\}}{\pi^2(2k+1)^2}\times \\ &\times\exp\left\{-\left(\kappa(2k+1)\pi/L\right)^2 t\right\} \end{aligned} \tag{31}$$

Here, $\kappa^2 = D_a B\Omega/k_B T$, $G = eZ\rho j/\Omega$, σ_T is the initial stress. Fig. 7 shows the evolution of distribution of the hydrostatic stress along the line, which yields a steady state linear stress distribution $\sigma_{Hyd}(x,\infty) = \sigma_T - eZ\rho j x/\Omega$, at $t \to \infty$:

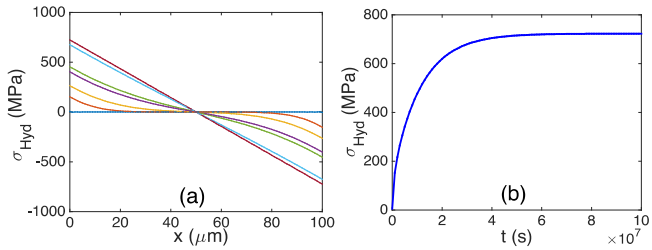

Fig. 6. Evolution of the hydrostatic stress (a) along the metal line loaded with DC current, and at the cathode end of line, (b) j = 5x10^{9}A/m^2, T = 400K.

As it was shown in [23], keeping just the slowest decaying term of the infinite series (31), provides an approximate void nucleation time t_{nuc} as an instant in time when σ reaches σ_{crit} at the line cathode end

$$t_{nuc} \approx \frac{L^2 k_B T}{D_a B\Omega}\ln\left\{\frac{eZ\rho jL/2\Omega}{\sigma_T + eZ\rho jL/2\Omega - \sigma_{crit}}\right\} \tag{32}$$

Equation (32) clearly demonstrates that in the case of $\sigma_{crit} > \sigma_T + \sigma_{EM}$, where $\sigma_{EM} = eZ\rho jL/2\Omega$, which is the Blech condition of immortality, [24]: $jL < 2\Omega(\sigma_{crit} - \sigma_T)/eZ\rho$, t_{nuc} diverges indicating the line immortality. When $\sigma_T > \sigma_{crit}$, the equation (32) yields the negative void nucleation time, which is the condition for stress voiding. Indeed, if the residual stress exceeds the critical stress needed for void nucleation, then a void will be nucleated without any electrical stressing. Representing t_{nuc}, given by (32), in the traditional form of the Black equation, $t_{nuc} = Aj^{-n}\exp\{-E_a/k_B T\}$, and extracting the current density exponent n and apparent activation energy E_a, confirms an existence of the discussed in literature dependencies of n and E_a on T_{test} and j by the fit between the

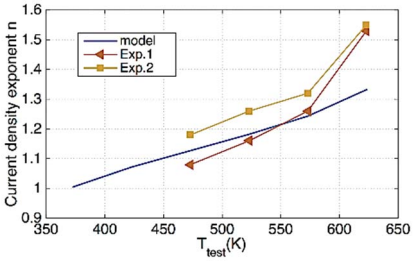

Fig. 7. Extracted dependency of n on T_{test} for T_{ZS}=723 K, σ_{crit}= 600MPa vs. experimental data: Exp. 1, [25], and Exp. 2, [26].

predicted dependency $n(T_{test})$ and the measurement results, shown in Fig. 7. Obtained increase in the activation energy E_a, [23], caused by the increase of the current density corresponds to the experimental observations, [25].

It should be mentioned, that everywhere above D_a is the effective atomic diffusivity, which is determined mainly by the

interfacial and GB diffusivities, [10]. Dependence of D_a on the grain size distribution demonstrates an additional to σ_{crit} parameter reflecting the statistical nature of the EM phenomenon.

It is obvious that a change in line resistivity will be initiated at t_{nuc}. Growing void increases the line resistivity and, at the end, when it occupies the entire cross section of the wire, pushes the electric current to flow through the highly resistive metal liners. A kinetics of the void volume evolution in 1D approximation was derived in [27]. Void nucleation occurs near the cathode edge of the line when the increasing with time tensile stress creates a condition for a stable growth of the preexisted process-induced flaws located at the metal/passivation interface. It means, the metal in the vicinity of the growing void is under essential tension, about σ_{crit}. Large stress gradient build in between the void surface, characterized by zero normal stress, and metal bulk pushes atoms to move from the void surface into the metal. A new BC for the void surface (void edge in 1D approximation) takes the form:

$$\frac{\partial \sigma}{\partial x}\left(l_{void},t\right)\approx\frac{\sigma\left(l_{void},t\right)}{\delta};\ 0<t<\infty \qquad (33)$$

Solution of the equation (30) with this new flux BC provides the kinetics of post-voiding stress evolution shown in the Fig. 8, a. Shown in Fig. 8, b the analytical solution for the void volume evolution $V_{void}(t)=V_{line}\int_0^L(\sigma(x,t)/B)dx$ can be found in [27]. It can be seen that 10% degradation of line resistance, which is calculated with $\rho_{TaN}=2.5\cdot10^{-6}\Omega m$, $\rho_{Cu}=3\cdot10^{-8}\Omega m$, $H=120nm$, and $h_{lin}=10nm$, caused by the growing void is developed in three order of magnitude shorter time (Fig. 8, b) than the time required for the void nucleation (Fig. 8, c).

Equation (30) can be used also for predicting the stress evolution in interconnect lines loaded with different kind of time-dependent electric stressing $j(t)$, such as AC and pulsed currents, [28]. General solution takes the form:

$$\sigma(x,t)=\sigma_T+\frac{4eZ\rho}{\Omega L}\kappa\sum_{n=0}^{\infty}Cos\frac{(2n+1)\pi x}{L}e^{-\kappa\frac{(2n+1)^2\pi^2}{L^2}t}\times \qquad (34)$$
$$\times\int_0^t j(t)e^{\kappa\frac{(2n+1)^2\pi^2}{L^2}\tau}d\tau$$

As an example, the Fig. 9 shows the current switch-off induced relaxation kinetics of stresses accumulated at the cathode end of line during $4x10^7$s of stressing by DC current with the density of $1x10^9$ A/m^2 at T = 373 K and 400 K.

IV. A Comparison of 1D and 2D/3D Predictions

We have demonstrated that the proposed 1D EM approximation can generate physically correct solutions for a number of important problems. Now we will examine a direct comparison between the predictions made with the simple 1D considerations and results obtained by 2D simulations.

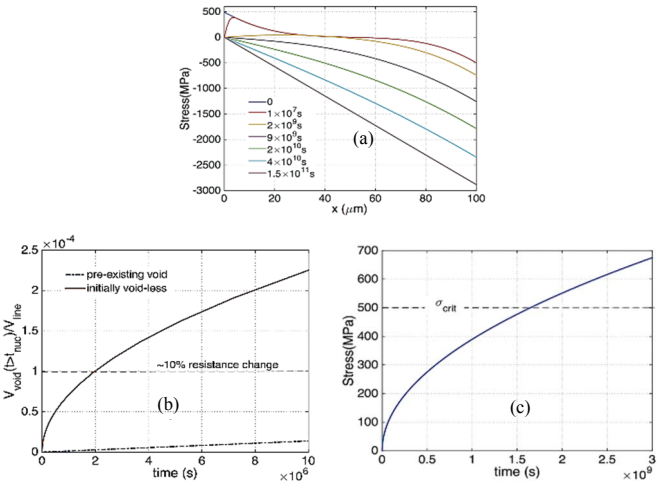

Fig. 8. Post-voiding evolution of the distribution of the hydrostatic stress along the metal line, (a). Void growth kinetics, (b); and the pre-voiding kinetics of the stress buildup at the cathode end of line, (c). For all cases: j=1x10^{10}A/m^2, T=400 K and $\sigma_T=0$, [27].

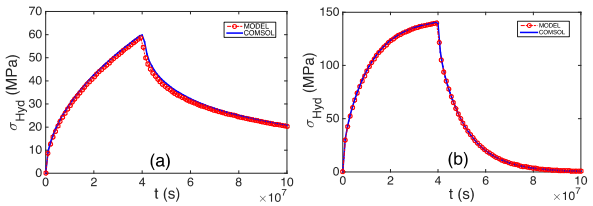

Fig. 9. Stress relaxation at T=373 K (a) and T=400 K (b), [28].

A simple 2D case of the metal line embedded into the rigid confinement, Fig. 10, shows quite different distributions of hydrostatic stresses inside grain interior and interface, which can be explained by different vacancy formation energies and diffusivities. 1D approximation provides a correct t_{nuc} by using the interfacial vacancy diffusivity, Fig. 10. At the same time, the correct 1D description of the void growth kinetics requires to use the vacancy diffusivity averaged across the line cross section. Fig. 11,a shows that 2D FEA-based simulation of the post-voiding evolution of stress occurring in a long interconnect line provides the results similar to what was obtained with 1D approximation, Fig. 8,a. A good fit between simulated kinetics of void volume evolution obtained with 1D and 2D FEA simulations is demonstrated in Fig 11, c and d.

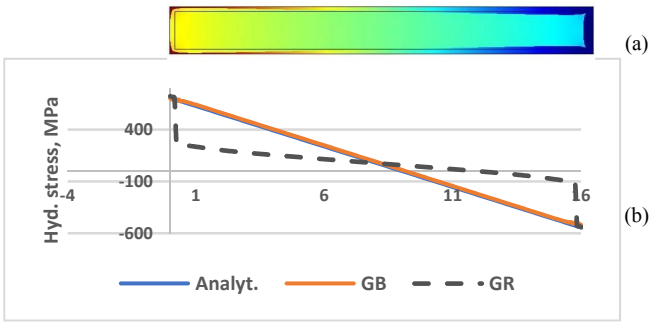

Fig. 10. Distributions of the hydrostatic stress and the interface displacement (scale factor is 150) caused by the applied DC voltage of 0.01V, (a); distributions of the simulated hydrostatic stress along the interface with a confinement and along the central line crossing the metal interior, (b).

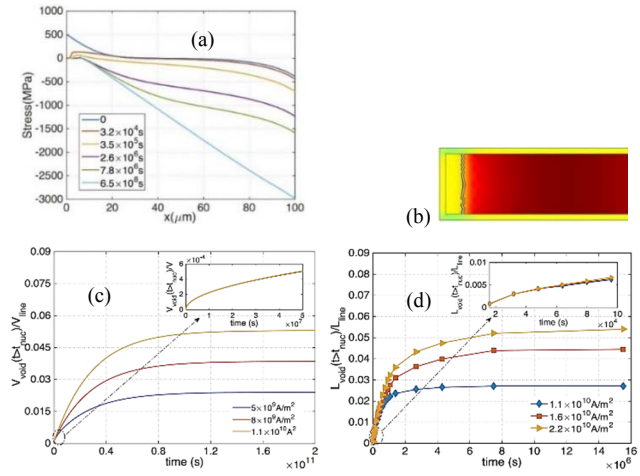

Fig. 11. Post voiding stress evolution with the time instances indicating the time elapsed since the void was nucleated, (a). Simulated void evolution, (b). Evolution of void volume obtained with 1D (c), and FEA (d) simulations.

Different type of problems, such as the effect of GB/IF diffusivities and GB orientations on void evolution, shown in Fig. 12, requires the employment of 2D/3D FEA simulations and cannot be properly addressed by 1D modeling.

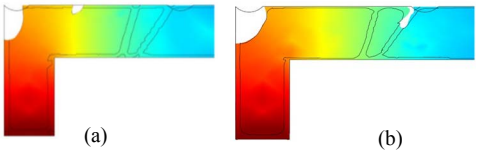

Fig. 12. Simulated growth of the line corner void caused by scavenging the vacancy flux and agglomerating with the small voids drifting along the top interface in two cases: the diffusion along the top interface prevails $D_{IF} >> D_{GB,}$ (a), the diffusion along the GB prevails $D_{IF} << D_{GB,}$ (b), [4].

All these examples demonstrate a good capability of 1D EM model to capture the EM induced degradation in one dimension-like metal segments. It means it can be employed for the EM assessment in large electrical circuits such as on-chip power grids.

V. Power Grid EM Cheking Using Physics-Based Models

Standard practice employed in the industry for the EM assessment is to break up a grid into isolated metal branches, assess the reliability of each branch separately using Black's model and then use the series model (earliest branch failure time) to determine the failure time for the whole grid. This approach is highly inaccurate, for at least three reasons. First, the fitting parameters obtained for Black's model under accelerated testing conditions are not valid at actual operating conditions, and this leads to significant errors in lifetime extrapolation, [26]. Second, Black's model ignores the material flow between branches. In today's mesh structured power grids, many branches within the same layer are connected and atomic flux can flow freely between the branches of an interconnect tree. As a result, if the individual branches happen to be short so that they are deemed immortal due to the Blech effect [24], then the tree would appear to be immortal, which is highly optimistic and can be entirely misleading for design. Finally, the third problem lies with the series model assumption. A series model is the case where a power grid is deemed to have failed as soon as the first of its branches has failed, typically due to an open circuit. However, modern power grids use a mesh structure. As such, there are many paths for the current to flow from the C4 bumps to the underlying logic, a characteristic we have referred above to as redundancy. Mesh power grids are in fact closer to (but not quite) a parallel system. As such, it is highly pessimistic to assume that a single branch failure will always cause the whole grid to fail. Thus, there is a need for a new EM checking approach that accurately models EM degradation using physics-based models, combined with a mesh model to account for redundancy, while being fast enough to be practically useful.

This novel approach has been developed recently, [29, 30]. While both teams have implemented similar physical models, the advanced numerical technique developed in [30] appears to be promising for EM assessment in power grids of large VLSI circuits. The developed in [30] approach consists of the decomposing the power grid into a number of interconnect trees, solving the set of PDEs (30) for all branches of each tree characterized by different current densities and geometries (length and width), and linking the solutions to each other through the proper BC at the segment junctions, which represent the continuity of stress and atomic fluxes. The latter secures an accurate calculation of stress evolution inside multi-segment tree. Fig. 13 shows the kinetics of stress evolution at all tree junctions and the evolution of the stress distribution across the 3-treminal tree shown in Fig. 14. An improved computational speed is achieved using an efficient filtering scheme and a fast predictor-based approach. This has been proved to have minimal impact on accuracy.

The extended Korhonen model starts out as a system of PDE coupled by the boundary laws, which are then scaled and discretized to reduce the model to a system of ordinary differential equations (ODE). The method then moves on to numerically solve the ODE system at successive time-points to track the stress evolution and find the corresponding time of void nucleation(s).

The random nature of EM degradation is accounted for using a Monte Carlo method. Successive samples of grid time-to-failure are found, until the estimate of the overall MTF has converged to satisfy user provided thresholds.

Computation speed is enhanced by using a filtering scheme that estimates upfront the set of trees that are most likely to impact the MTF assessment of the grid, with minimal impact on accuracy. The process also includes a predictive scheme that allows for faster MTF estimation by extrapolating the solution (stress curve) obtained from a few initial time-points.

The developed approach was tested on a number of IBM power grid benchmarks, [31], on a quad-core 3.4GHz Linux machine with 32GB of RAM. The MTFs estimated using the physics-based approach were on average 3x longer than those based on a (calibrated) Black's model, supporting the claim that Black's model is not accurate enough for modern power grids and confirming the need for physical models. Having achieved a run-time of less than three hours for the largest grid

(700K nodes), this approach has been demonstrated as suitable for large VLSI circuits.

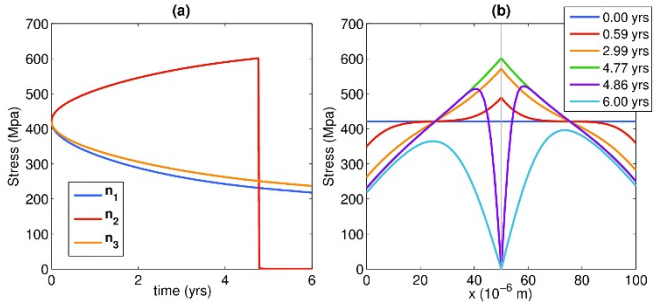

Fig. 13. Evolution of stress at junctions with time, (a) and stress profile evolution with time, (b). Here L_1=L_2=50mm, and j_1=-j_2=6e9 A/m^2, [30].

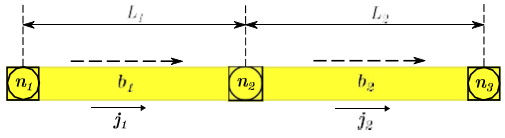

Fig. 14. A simple 3-terminal tree.

VI. CONCLUSIONS

We discussed the state of the art physics-based analytical modeling and numerical analysis approaches currently employed for the prediction and description of EM induced degradation of individual interconnect metal lines and on-chip power grids. We demonstrated a general model of the mechanical stress evolution caused by an electric current driven redistribution of vacancies and plating atoms, which initiates the growth of preexisted crystal imperfections such as micro caverns and interfacial/inter-granular delaminating. Different kind of analytical/numerical techniques employed for analysis of EM degradation in different cases characterized by the scales varying from the size of an individual line to the multibillion segment power grids were discussed.

REFERENCES

1. A. S. Oates, and M. H. Lin, "Electromigration Failure Distributions of Cu/Low-*k* Dual- Damascene Vias: Impact of the Critical Current Density and a New Reliability Extrapolation Methodology", *IEEE Trans. Device Mater. Rel*., vol. 9, pp. 244-254, 2009.
2. B. I. Shklovskii and A. L. Efros, *Electronic Properties of Doped Semiconductors*. Springer-Verlag, 1984.
3. J. B. Bernstein, M. Gurfinkel, et al., "Electronic circuit reliability modeling", *Microelectr.. Reliability*, vol. 46, pp. 1957–1979, 2006.
4. V. Sukharev, A. Kteyan, et al., Microstructure Effect on EM-Induced Degradations in Dual Inlaid Copper Interconnects, *IEEE Trans. Device Mater. Rel*., vol. 9, pp. 87–97, 2009.
5. A. Einstein, "Über die von der molekularkinetischen Theorie der Wärme geforderte Bewegung von in ruhenden Flüssigkeiten suspendierten Teilchen". *Annalen der Physik* (in German), vol. 322, pp. 549–560, 1905.
6. P. S. Ho and T. Kwok, Electromigration in metals, *Rep. Prog. Phys*., vol. 52, pp. 301–348, 1989.
7. C. Herring, Diffusional viscosity of a polycrystalline solid, *J. Appl. Phys*., vol. 21, pp. 437-445 1950.
8. V. Sukharev, E. Zschech, et al., "A model for electromigration-induced degradation mechanisms in dual-inlaid copper interconnects: Effect of microstructure," *J. Appl. Phys*., vol. 102, no. 5, pp. 053 505- 1–053 505-14, 2007.
9. M. A. Korhonen, P. Borgesen, et al., "Stress evolution due to electromigration in confined metal lines," *J. Appl. Phys.*, vol. 73, pp. 3790–3799, Apr. 1993.
10. Z. Suo, "Reliability of Interconnect Structures" in *Volume 8: Interfacial and Nanoscale Failure*, edited by W. Gerberich, W. Yang, Comprehensive Structural Integrity, Elsevier, Amsterdam, 2003, pp. 265-324.
11. R. J. Gleixner, B. M. Clemens, et al., ``Void Nucleation in Passivated Interconnect Lines: Effects of Site Geometries, Interfaces, and Interface Flaws," *J. Mater. Res.*, vol. 12, pp. 2081-2090, 1997.
12. M. W. Lane, E. G. Liniger, et al., "Relationship between interfacial adhesion and electromigration in Cu metallization", *J. Appl. Phys.*, vol. 93, pp. 1417-1421, 2003.
13. Paul G. Shewmon, *Diffusion in Solids*, McGraw-Hill, 1963.
14. M J. Aziz, "Thermodynamics of diffusion under pressure and stress: Relation to point defect mechanisms", *Appl. Phys. Lett*., vol. 70, pp. 2810-2812, 1997.
15. R. Kirchheim, "Stress and electromigration in Al-lines of integrated circuits," *Acta Metall. Mater*., vol. 40, no. 2, pp. 309–323, 1992.
16. M. E. Sarychev, Yu. V. Zhitnikov, et al., "General model for mechanical stress evolution during electromigration", *J. Appl. Phys*., vol. 86, pp. 3068-3075, 1999.
17. L. D. Landau and E. M. Lifshitz, *Theory of elasticity*, Pergamon Press, 1970.
18. V. Timoshenko and J. N. Goodier, *Theory of Elasticity*, New York: McGraw-Hill, 1951.
19. D. Bhate, A. Bower, et al., "A phase field model for failure in interconnect lines due to coupled diffusion mechanisms", *J. Mech. Phys. of Solids*, vol. 50, pp. 2057-2083, 2002.
20. V. Sukharev, R. Choudhuty, et al., "Physically-based simulation of the early and long-term failures in the copper dual damascene interconnect", *Integrated Reliability Workshop Final Report, 2003 IEEE International*, pp. 80-85, 2003.
21. J. J. Clement, "Reliability Analysis for Encapsulated Interconnect Lines under DC and Pulsed DC Current Using A Continuum Electromigration Transport Model," *J. Appl. Phys*., vol. 82, pp. 5991–6000, 1997.
22. S.P. Hau-Riege and C.V. Thompson, "The effect of mechanical properties of the confinement material electromigration in metallic interconnect", *J. Mater. Sci*., vol. 15, pp. 1797-1802, 2000.
23. V. Sukharev, "Beyond Black's equation: Full-chip EM/SM assessment in 3D IC stack", *Microelectr.. Eng.*, vol. 120, pp. 99-105, 2014.
24. I. A. Blech, "Electromigration in thin aluminum films on titanium nitride," *J. Appl. Phys*., vol. 47, no. 4, pp. 1203–1208, 1976.
25. M. Hauschildt, G. Talut, et al, Electromogration void nucleation and growth analysis using large-scale early failure statistics, Book of Abstracts, *12th International Workshop on Stress-Induced Phenomena in Microelectronics*, May 2012, Japan.
26. M. Hauschildt, C. Hennesthal, et al. "Electromigration Early Failure Void Nucleation and Growth Phenomena in Cu and Cu(Mn) Interconnects", *IEEE Int. Reliab. Phys. Symp.* Proc. (2013) 2C.1.1-6.
27. V. Sukharev, A. Kteyan, et al., "Postvoiding stress evolution in confined metal lines", *IEEE Trans. Device Mater. Rel*., vol. 16, pp. 50–60, 2016.
28. V. Sukharev, X. Huang , et al., "Electromigration induced stress evolution under alternate current and pulse current loads", *J. Appl. Phys*., vol. 118, pp. 034504, 2015.
29. X. Huang, A. Kteyan, et al., "Physics-based electromigration models and full-chip assessment for power grid networks", *IEEE Trans. Comput.-Aided Design Integr. Circuits Syst.*, vol. 35, pp. 1848-1861, 2016.
30. S. Chatterjee, V. Sukharev, et al., "Fast Physics-based Electromigration Checking for On-die Power Grids," in *Proc. of the 35th Int. Conf. on Computer-Aided Design*, Nov. 2016, pp. 110:1–110:8.
31. S. R. Nassif, "Power grid analysis benchmarks," in *ASP-DAC*, 2008, pp. 376–381.